4. S. Fields and R. Sternglanz, *Trends Genet.* **10**, 286 (1994).
5. The pLexA-TAK1ΔN plasmid comprises the TAK1ΔN coding sequence (TAK1 residues 21 to 579) (*2*) inserted in frame into pBTM116 [A. B. Vojtek, S. M. Hollenberg, J. A. Cooper, *Cell* **74**, 205 (1993)]. The yeast two-hybrid system was used to identify proteins encoded by a human brain cDNA library that interact with TAK1ΔN. The two hybrids were expressed in a *Saccharomyces cerevisiae* strain L40 (*LYS2::lexA-HIS3*) that contains an integrated reporter construct in which a binding site for the LexA protein was placed upstream of the yeast *HIS3* coding region. If the two hybrid proteins interact, then transactivation of the reporter construct occurs and the yeast cells can grow in the absence of histidine (SC-His). The LexA-TAK1ΔN fusion protein alone induced sufficient *HIS3* expression to allow growth in the absence of exogenous histidine. However, histidine auxotrophy could be reestablished by growing cells in the presence of 40 mM 3-aminotriozole, a chemical inhibitor of the *HIS3* product, imidazole glycerol dehydrogenase [G. M. Kishore and D. M. Shah, *Annu. Rev. Biochem.* **57**, 627 (1988)].
6. K. Irie *et al.*, *Science* **265**, 1716 (1994).
7. The pheromone-stimulated MAPK pathway consists of the Ste11p, Ste7p, and either Fus3p or Kss1p kinases, which correspond to MAPKKK, MAPKK, and MAPK, respectively. These yeast protein kinases act sequentially to transmit a signal to the transcription factor Ste12p, which activates transcription of mating-specific genes such as *FUS1* [I. Herskowitz, *Cell* **80**, 187 (1995); D. E. Levin and B. Errede, *Curr. Opin. Cell Biol.* **7**, 197 (1995); J. Schultz, B. Ferguson, G. F. Sprague Jr., *Curr. Opin. Genet. Dev.* **5**, 31 (1995)]. The *FUS1p::HIS3* reporter gene, which comprises the *FUS1* upstream activation sequence joined to the *HIS3* open reading frame, allows signal activity in a *his3Δ FUS1p::HIS3* strain to be monitored by the ability of cells to grow on SC-His medium (His phenotype). A *his3Δ ste11Δ FUS1p::HIS3 STE7^{P368}* (Pro substitution at Ser^{368}) strain has a His$^-$ phenotype (*6*). Expression of mammalian TAK1ΔN, but not TAK1, in this strain confers a His$^+$ phenotype (*2*). Thus, the activated form of TAK1 can substitute for Ste11p activity in a Ste7^{P368}-dependent manner.
8. The DNA sequence that encodes the HA epitope recognized by the monoclonal antibody 12CA5 was attached in frame to the DNA encoding the COOH termini of TAK1 and TAK1(K63W) by the polymerase chain reaction (PCR). All constructs were expressed from the *TDH3* promoter. The TAB1 expression plasmid, pGAP-HTH9M, encodes the COOH-terminal 68 amino acids of TAB1. The coding sequence for the COOH-terminal 68 amino acids of TAB1 was amplified by PCR with a 5′ primer (5′-GAGAATTCATGCGGCAAAGC-3′) incorporating an Eco RI site and an ATG codon, and a 3′ primer (5′-GGGTCGACTACGGTGC-3′) incorporating a Sal I site. A 240–base pair Eco RI–Sal I fragment generated by PCR was inserted into the Eco RI–Sal I gap of YEpGAP112, a multicopy *TRP1* plasmid that contains the *TDH3* promoter [H. Banno *et al.*, *Mol. Cell. Biol.* **13**, 4745 (1993)], to generate pGAP-HTH9M.
9. The truncated TAB1 cDNA obtained from the yeast two-hybrid system was used as a probe to screen a human kidney cDNA library (Clontech). The 5′ end of TAB1 mRNA was determined by 5′ rapid amplification of cDNA ends with 5′-RACE-Ready cDNA (Clontech). The nucleotide sequence (CCAAGATGG) at the putative NH_2-terminal end of the coding sequence corresponds to the Kozak consensus [M. Kozak, *J. Cell Biol.* **108**, 229 (1989)], and there are no upstream ATG codons.
10. S. Ohta *et al.*, *FEBS Lett.* **314**, 356 (1992).
11. The full-length TAB1 cDNA was subcloned into the pCS2MT vector [D. L. Turner and H. Weintraub, *Genes Dev.* **8**, 1434 (1994)], which encodes six copies of the MYC epitope (LEQKLISEEDLN) (*16*) recognized by the monoclonal antibody 9E10. In the resulting plasmid, pCS2MT-TAB1, DNA encoding the MYC epitope tag was attached in frame to the DNA sequence corresponding to the NH_2-terminus of TAB1. The pCS2MT-TAB1 plasmid was digested with Bam HI and Xba I, and the resulting fragment was isolated and inserted into the Eco RI–Xba I sites of the mammalian expression vector pEF, in which expression is controlled by the human elongation factor 1α (EF1α) gene promoter.
12. M. R. Keeton, S. A. Curriden, A.-J. Zonneveld, D. J. Loskutoff, *J. Biol. Chem.* **266**, 23048 (1991).
13. M. Abe *et al.*, *Anal. Biochem.* **216**, 276 (1994).
14. The TAB1 expression plasmid, pEF-TAB1, contains the full-length TAB1 coding sequence under the control of the EF1α gene promoter. This plasmid was generated by cleaving the pEF vector with Eco RI and inserting the Eco RI fragment from pBS-TAB1, which itself was generated by subcloning of the TAB1 cDNA into the Eco RI site of pBS.
15. K. Yamaguchi, K. Irie, K. Matsumoto, unpublished data.
16. Abbreviations for the amino acid residues: A, Ala; C, Cys; D, Asp; E, Glu; F, Phe; G, Gly; H, His; I, Ile; K, Lys; L, Leu; M, Met; N, Asn; P, Pro; Q, Gln; R, Arg; S, Ser; T, Thr; V, Val; W, Trp; and Y, Tyr.
17. Yeast strain L40 was cotransformed with (i) an expression vector encoding full-length TAK1 or a deletion construct fused to the LexA DNA binding domain and (ii) pGAD-TAB1 or pGAD-TAB2. Interaction between fusion proteins expressed by the specified plasmids was demonstrated by the ability of the yeast cells to grow on plates of SC−His containing 40 mM 3-aminotriozole. Each deletion construct of TAK1 was generated from the full-length TAK1.
18. Strain SY1984-P is SY1984 (*his3Δ ste11Δ FUS1p::HIS3*) transformed with plasmid pNC318-P368, which contains the *STE7^{P368}* allele under the control of the *CYC1* promoter (*6*). Plasmids pNV11-HU11 and pNV11-HU11F express, under the control of the *TDH3* promoter, TAK1ΔN and full-length TAK1, respectively (*2*).
19. Yeast cells (60-ml culture) were grown to an optical density at 600 nm of 0.8. Cell extracts were prepared with a lysis buffer as described (*6*) and centrifuged for 30 min at 100,000*g*. The supernatant was subjected to immunoprecipitation with antibodies to HA. Briefly, a portion (300 μl) of the supernatant was mixed with 2 μl of antibodies and 90 μl of protein A–Sepharose (Pharmacia), and the immune complex was washed three times with lysis buffer and assayed for kinase activity (*2*). Immunoblot analysis of each immunoprecipitate with monoclonal antibody 12CA5 to HA demonstrated that approximately the same amount of TAK1-HA or TAK1(K63W)-HA was recovered in each sample, indicating that TAB1 expression did not affect the amount of TAK1 expressed.
20. H. Shibuya *et al.*, *Nature* **357**, 700 (1992).
21. H. Shibuya *et al.*, *Mol. Cell. Biol.* **14**, 5812 (1994).
22. Transfection efficiency was normalized by cotransfection with the pXeX-β-Gal vector [A. D. Johnson and P. A. Krieg, *Gene* **147**, 223 (1994)] in all luciferase reporter experiments. The β-galatosidase assay was performed as described by the manufacturer (Clontech) with the cell lysates prepared for luciferase assay.
23. A 1.3-kb Eco RI–Hinc II fragment of pBS-TAB1 (*14*) that encodes amino acids 1 to 418 of TAB1 was subcloned into the pKT10 vector to generate pKT10-TAB1(1–418). The pEF-TAB1(1–418) plasmid was generated by cleaving the pEF vector with Eco RI and Sal I and inserting the Eco RI–Sal I fragment from pKT10-TAB1(1–418).
24. We thank M. Abe, B. Errede, A. Johnson, and D. Turner for materials; R. Ruggieri and R. Yu for critical reading of the manuscript; and H. Wang and J. Reed for helpful discussions and sharing data before publication. Supported by a special grant for Advanced Research on Cancer from the Ministry of Education, Culture, and Science of Japan (to K.M.).

12 December 1995; accepted 4 March 1996

Requirement for Cholinergic Synaptic Transmission in the Propagation of Spontaneous Retinal Waves

Marla B. Feller,* David P. Wellis, David Stellwagen, Frank S. Werblin, Carla J. Shatz

Highly correlated neural activity in the form of spontaneous waves of action potentials is present in the developing retina weeks before vision. Optical imaging revealed that these waves consist of spatially restricted domains of activity that form a mosaic pattern over the entire retinal ganglion cell layer. Whole-cell recordings indicate that wave generation requires synaptic activation of neuronal nicotinic acetylcholine receptors on ganglion cells. The only cholinergic cells in these immature retinas are a uniformly distributed, bistratified population of amacrine cells, as assessed by antibodies to choline acetyltransferase. The results indicate that the major source of synaptic input to retinal ganglion cells is a system of cholinergic amacrine cells, whose activity is required for wave propagation in the developing retina.

Spontaneous activity generated in immature circuits is present in various regions of the central nervous system (*1–3*) and participates in the development and differentiation of synaptic circuitry (*4*). Long before the onset of vision, mammalian retinal ganglion cells exhibit spontaneous, periodic bursts of action potentials (*5–7*). At this early stage of development, blockade of neural activity prevents the segregation of retinal ganglion cell axons into appropriate eye-specific layers within their thalamic target nucleus (*8*), and modification of retinal activity at later ages alters the development of retinal ganglion cell dendrites and receptive fields (*9*).

The spatial pattern of activity among neighboring ganglion cells resembles waves that periodically propagate across the ganglion cell layer (*6, 10*). To investigate the

Howard Hughes Medical Institute and Department of Molecular and Cell Biology, University of California, Berkeley, Berkeley, CA 94720–3200 USA.

*To whom correspondence should be addressed at 221 Life Sciences Addition, University of California, Berkeley, CA 94720–3200, USA. E-mail: marla@violet.berkeley.edu

suggested possibility that an early functional network consisting of both amacrine and ganglion cells is involved in the generation of retinal spontaneous activity (*10*), we used both whole-cell recording techniques and optical imaging of fura-2–stained whole-mount retinae from newborn ferrets (*11*).

Fluorescence imaging revealed that each wave does not propagate across the entire retina but is spatially restricted to a discrete region, which we call a domain (Fig. 1) (*12*). The domains vary in shape; some appear to fan out from a central region (Fig. 1B, top row, first minute: blue and purple waves), and others propagate with a linear wave front (Fig. 1B, top row, first minute: red and orange waves). Waves can originate from the center of the field of view, indicating that the waves are not initiated simply at tissue edges or discontinuities. [These characteristics are illustrated in the first segment of the videotape that accompanies this report (*12a*, segment 1).] Similar patterns of activity were recorded from 89 retinas.

Over a prolonged recording period (Fig. 1B, top row), a mosaic emerges indicating that over time, the entire retina becomes "tiled" by individual domains (Fig. 1B, bottom row). Also the boundaries between individual domains are not fixed. For example, the region covered by the purple domain in the first minute of recording in Fig. 1B (top row) is subsequently covered by four smaller domains in the last minute of recording.

On a time scale of less than 1 min, however, neighboring wave domains do not invade each others' borders (Fig. 1B), whereas, as mentioned above, over a longer period (4 min) the overlap is substantial. Thus, there appears to be a refractory period following activation of a group of cells during which they cannot participate in another wave. To examine this possibility, we computed the difference in initiation times of neighboring pairs of waves that did not invade each other's territory versus those pairs that did invade each other's territory. The results from one retina (Fig. 2A) indicated that when neighboring waves initiated within 45 s of each other, no domain overlap occurred. In six retinas, refractory periods of 40 to 60 s were observed by this method.

We next examined the boundaries of waves generated artificially by depolarization. Pressure ejection of K^+ from a micropipette can depolarize a small group of cells that can then generate a propagated wave (*12a*, segment 2; *13*). A refractory period analysis on the evoked domains indicated that, whenever a propagated wave resulted, the interval between consecutive evoked or spontaneous waves was more than 50 s (Fig. 2B). In all three retinas examined, this interval was identical to the refractory period derived by examining all the spontaneously generated waves occurring in the same field of view (Fig. 2B, lower histogram). These observations indicate that the geometry of individual domains is dynamic and not due to the activation of invariant groups of cells. Rather, the past history of excitability in the retina is likely to dictate the patterning of the domains.

To gain insight into the mechanism of generation and propagation of the waves, we monitored the membrane properties of retinal ganglion cells with whole-cell patch clamp recordings (*14*). Voltage clamp recordings revealed periodic barrages of postsynaptic currents (PSCs) (Fig. 3A) that appear to be composed of many individual PSCs. The interval between compound PSCs in this case was 110 ± 44 s, closely matching the period between waves (115 ± 48 s) optically recorded from the surrounding tissue. Similar periodic compound PSCs were observed from more than 85% of the recorded cells (120 of 135, $n = 56$ retinae).

These observations suggest that ganglion cells receive synaptic inputs that are generated as waves pass through the area, a possibility supported by simultaneous whole-cell recording from a single ganglion cell and fluorescence imaging of the surrounding retina (Fig. 3B). Eight ganglion cells in four different retinas were recorded; 94% of the waves that traversed the region generated a compound PSC in the recorded cell, and nearly (92%) every compound PSC was accompanied by a detectable change in fluorescence. Thus, there is a correspondence between the periodic compound PSCs and the increases in intracellular calcium concentration

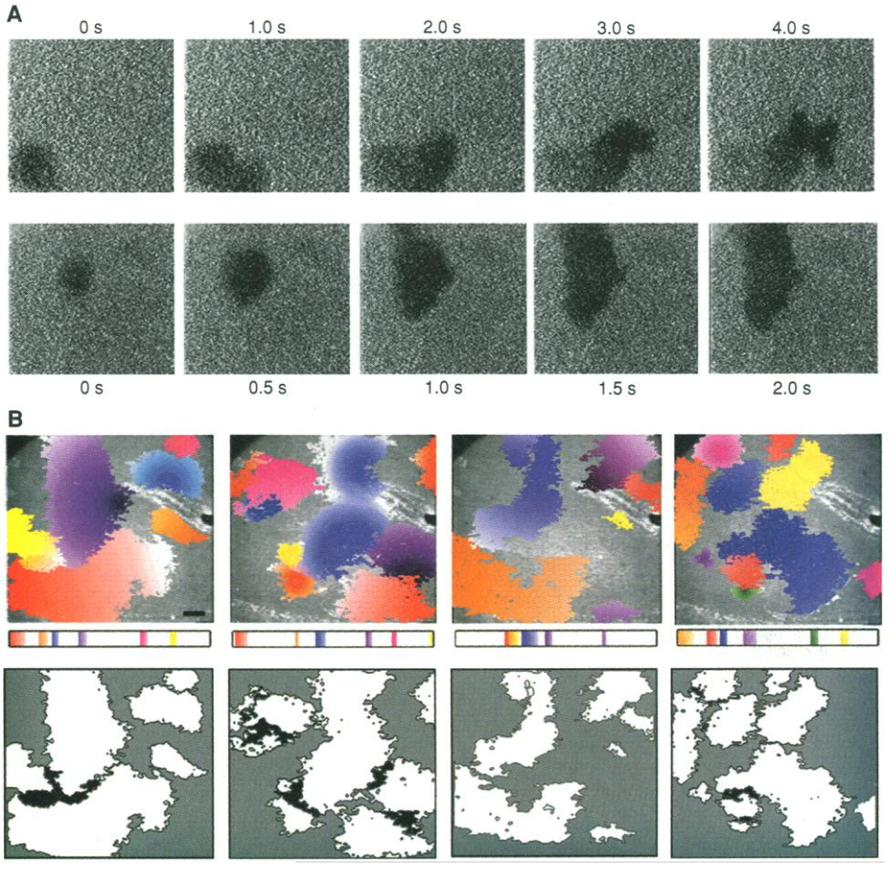

Fig. 1. Spontaneous waves measured with fluorescence imaging in a P2 ferret retina stained with fura-2AM. (**A**) Time evolution of two separate waves, occurring 30 s apart. First wave (top): Successive 1-s intervals from a real-time movie of the fura-2 fluorescence decrease associated with increased $[Ca^{2+}]_i$ evoked by waves (*12*). Second wave (bottom): Successive 0.5-s intervals. (**B**) The spatial and temporal properties of 30 consecutive waves observed over a 4-min recording period. (Top) Four consecutive minutes of activity. Background: fluorescence image (380-nm excitation). Different colors correspond to individual domains with a color-coded time bar below each frame to indicate the time of propagation of each event. The red domain of the first frame corresponds to the wave shown in the top sequence in (A); the purple domain corresponds to the wave in the bottom sequence. The gradation of color within each event corresponds to the direction of propagation of the wave, with the most saturated color corresponding to the initiation zone. (Bottom) Outline of each of the domains shown on the top, with the regions that participated in more than one wave shown in black. Scale bar, 100 μm.

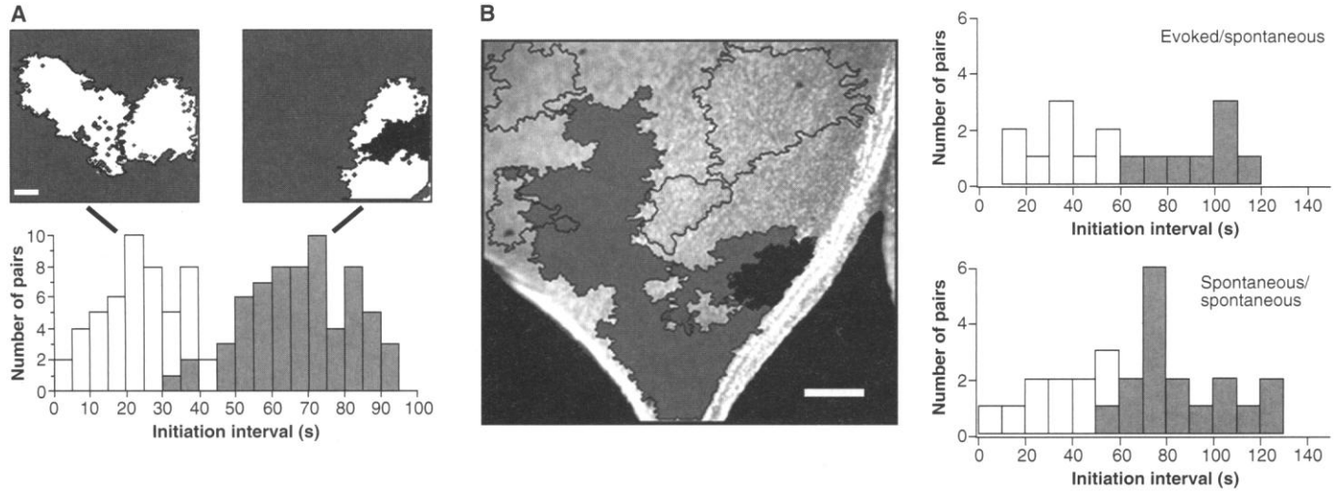

Fig. 2. Refractory period analysis. (**A**) Distribution of the difference in the initiation times of neighboring waves recorded from a P7 ferret retina. In all, 115 neighboring waves (any two whose domains abutted or overlapped) were considered. The neighboring pairs were placed in one of two categories depending on whether (i) a wave in one domain was unable to invade the other's territory (the region of overlap was less than 10% of the total area of either domain), or (ii) a wave in one domain could invade the territory of the other (the region of overlap was more than 10%). Only neighboring waves that had initiation times within 90 s of each other were considered. An example of a pair of waves that did not invade each other's territories is shown on the upper left; a pair of waves that did invade is shown on the right, with the overlap region indicated in black. The refractory period is the time covered by the histogram distribution of the first category (open bars), which in this experiment is about 45 s. Scale bar, 100 μm. (**B**) Waves can be induced by puffs of ACSF containing 120 mM K^+ (*13*). On the left are domains of two waves induced by pressure ejection of K^+ (gray). Neighboring waves that occurred spontaneously within 2 min of the first puff (open areas) are also shown. The black region represents the spatial extent of the K^+-induced direct depolarization that was determined by applying a second puff of K^+ during the refractory period of the surrounding tissue. On the right are the initiation interval histograms of spontaneous waves compared to puff (top, n = 17 wave pairs) or to other spontaneous waves (bottom, n = 29 wave pairs). Scale bar, 100 μm.

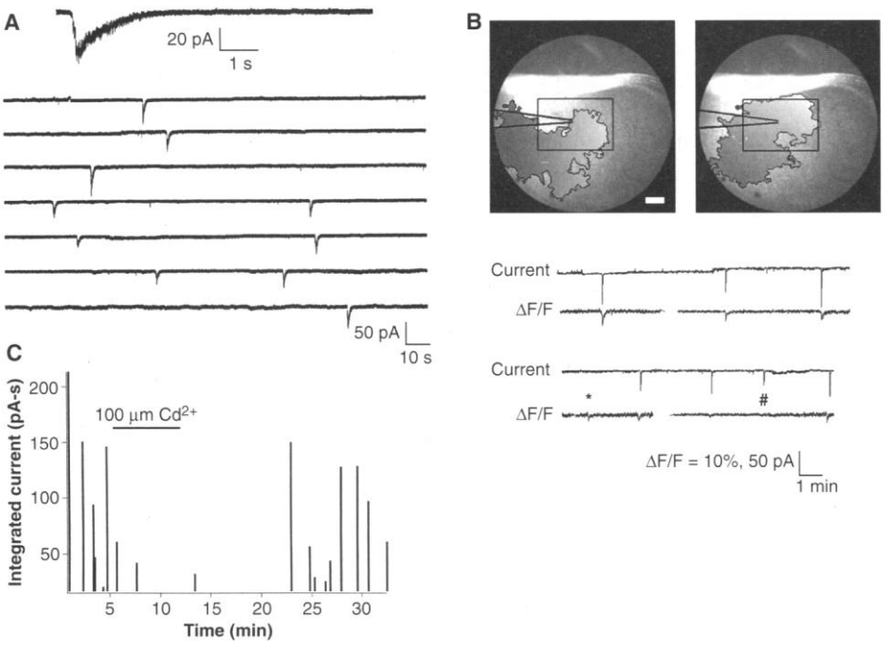

Fig. 3. Periodic compound PSCs measured in ganglion cells. (**A**) Continuous whole-cell voltage clamp recording for 28 min; an expansion of 5 s surrounding a single compound PSC (top). (**B**) Top: spatial extent of the first two waves passing through the region surrounding a whole-cell recording electrode. Scale bar (lower right), 200 μm. (Bottom) Continuous simultaneous recordings for 20 min [top traces correspond to the voltage clamp recordings; bottom traces correspond to the fractional change in fura-2 fluorescence ($\Delta F/F$) associated with waves averaged over the 0.5 mm^2 surrounding the recording electrode]. The breaks in the fluorescence trace correspond to readjustments of camera gain to compensate for fading of the fura-2 dye. *, Wave that did not involve the cell from which we were recording. #, Compound PSC where the fluorescence change induced by the associated wave was either below the sensitivity of the optical technique or not there at all. (**C**) Compound PSCs were blocked by a bath application of 100 μM Cd^{2+}. Each vertical line represents the magnitude of the current integrated over a 5-s period surrounding each barrage. Only values above 1 pA·s were included.

($[Ca^{2+}]_i$) as waves traversed the region, suggesting that they both reflect the same phenomenon. In addition, when 50 to 100 μM Cd^{2+} was added to the bath during whole-cell recordings (five cells, two retinae) the periodic compound PSCs were essentially abolished (Fig. 3C), as would be expected if currents are generated by means of synaptic transmission.

Pharmacological studies of the developing mammalian retina have shown that, even though ganglion cells receive spontaneous miniature synaptic inputs that can be blocked by glutamate antagonists at early ages (*15*), the retinal waves are not blocked by these agents (*7*, *10*). Other candidate transmitter systems in the retina at early ages include the transmitters contained within amacrine cells. Studies in the developing retinas of rabbit and turtle have shown that the periodic bursting of retinal ganglion cells can be modulated by cholinergic agonists and antagonists (*16*), implying a possible role for cholinergic amacrine cells in the generation and propagation of retinal waves.

Bath application of *d*-tubocurarine, a nicotinic acetylcholine receptor (nAChR) antagonist, reversibly blocked the periodic compound PSCs recorded from retinal ganglion cells (Fig. 4A). However, α-bungarotoxin, an antagonist that blocks a subset of nAChRs, had no effect on the periodic increases in $[Ca^{2+}]_i$ (Fig. 4B), whereas curare abolished them entirely as expected from the

whole-cell results. In addition, bath application of nicotine blocked the periodic compound PSCs (10 μM, three cells, three retinas) and the periodic increases in $[Ca^{2+}]_i$ (four retinas), most likely through desensitization of the nAChR (*17*). These observations implicate the α-bungarotoxin–insensitive subtype of neuronal nAChR (*18*), which is present in the vertebrate retina (*19*), in the generation of the waves. In addition, we attempted to induce waves in the presence of curare by pressure ejection of K^+ (as in Fig. 2B). Although pressure ejection of K^+ could always induce a local depolarization of ganglion cells close to the pipette, the excitation did not evoke a propagating wave when curare was present in the bath (Fig. 4C, five retinas). Thus, cholinergic synaptic transmission is required for the propagation of the waves. Consistent with this conclusion, waves could also be produced by pressure ejection of acetylcholine (ACh) or nicotine (*12a*, segment 3). However, consecutive waves were not induced as reliably as with K^+ because successive pressure ejection of nicotine did not directly depolarize cells sufficiently to generate a detectable increase in $[Ca^{2+}]_i$, presumably as a result of receptor desensitization. We conclude that depolarization through activation of nAChRs is sufficient to start a wave; however, these experiments do not permit us to conclude that the waves are naturally initiated by ACh.

To determine whether retinal ganglion cells receive direct cholinergic input, we next examined the periodic compound PSCs recorded from ganglion cells for current-voltage characteristics similar to those of α-bungarotoxin–insensitive neuronal nAChRs, which typically show inward rectification with an inflexion near 0 mV (*18*). To our surprise, inward currents recorded at −60 mV could be reversed at −20 mV (Fig. 5), suggesting that another conductance is also activated during waves. A likely candidate is a α-aminobutyric acid (GABA)–mediated chloride conductance because most amacrine cells contain and release GABA (*20*); in fact, SR95531, a selective and potent $GABA_A$ receptor antagonist for retinal ganglion cells (*21*), significantly reduced the outward current measured at depolarizing holding potentials (Fig. 5A), revealing an underlying inward rectifying current (Fig. 5B) (*22*).

In contrast, SR95531 had no effect on the periodicity of the compound PSCs, indicating that the $GABA_A$ antagonist had no effect on the generation of the waves. In addition, imaging experiments showed that the increases in $[Ca^{2+}]_i$ associated with the waves persisted in the presence of SR95531 with no detectable change in the periodicity of the waves (n = 4). Our observations taken together indicate that retinal ganglion cells receive direct cholinergic and GABAergic inputs, but that only the cholinergic inputs are required for the wave generation (*23*).

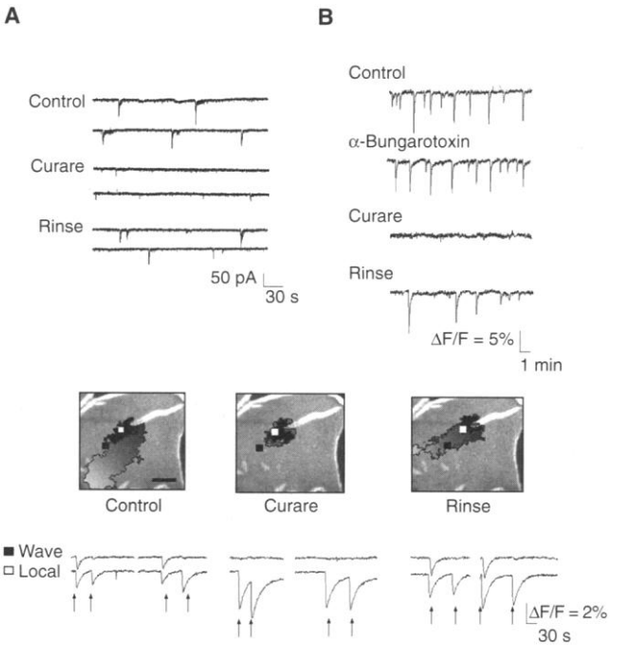

Fig. 4. Effects of *d*-tubocurarine on spontaneous and evoked waves. (**A**) Continuous whole-cell recordings from a ganglion cell in ACSF and in ACSF containing 100 μM *d*-tubocurarine (n = 8 cells, 6 retinas). (**B**) $\Delta F/F$ averaged over a (100 μm)^2 area of tissue in ACSF, in ACSF containing 200 nM α-bungarotoxin (n = 2 retinas), and in ACSF containing 100 μM d-tubocurarine (n = 10 retinas). (**C**) (Top) Superposition of two consecutive K^+-induced waves on the fura-2 fluorescence image of the ganglion cell layer. The second application of K^+ occurs within the refractory period of the tissue and therefore cannot induce a wave (Fig. 2B). Black region represents the spatial extent of the K^+-induced local depolarization. (Bottom): $\Delta F/F$ averaged over (100 μm)^2 at two sites (squares adjacent to and 500 μm from the puffer electrode). A longer puff (200 ms compared to 100 ms) was used in the presence of curare in order to assure a strong depolarization. Scale bar, 500 μm.

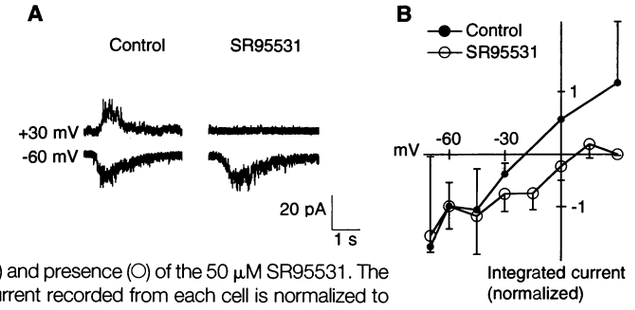

Fig. 5. Conductances activated in retinal ganglion cells during a wave. (**A**) Spontaneous compound PSC recorded in a single ganglion cell held at −60 mV and at +30 mV in the absence and presence of 50 μM SR95531, a $GABA_A$ antagonist. (**B**) Summary plot of the IV characteristics of the periodic compound PSCs in the absence (●) and presence (○) of the 50 μM SR95531. The magnitude of the integrated current recorded from each cell is normalized to the average value recorded for that cell at V_H = −60 mV. Each point corresponds to the normalized magnitude recorded at a given holding potential averaged across cells (in control ACSF, 56 compound PSCs were recorded at six different holding potentials between −70 mV and +30 mV in seven cells; in SR95531, 85 compound PSCs at eight different holding potentials from nine different cells). The error bars correspond to the standard deviation.

In adult and developing retinas of many vertebrates, the only source of ACh is found in a subclass of amacrine cells, known as the starburst amacrines (*24*). These starburst amacrines make synaptic connections with ganglion cells (*16*, *25*, *26*) and with other amacrines (*26*, *27*), and they contain and co-release ACh and GABA (*28*). The cells that supply the cholinergic inputs to the ganglion cells in retinas of newborn ferrets were identified by immunohistochemical staining for choline acetyltransferase (ChAT) (*29*). Retinal whole mounts immunostained for ChAT revealed a uniform mosaic (Fig. 6A) of amacrine cells, confirmed in sectioned retinas (Fig. 6B) by the presence of a bistratified immunostained population, with one layer of cell bodies in the amacrine cell layer and the other displaced into the ganglion cell layer. The processes of the cells form two distinct strata in the inner-plexiform layer. This characteristic bistratified distribution and small soma size of the ChAT-positive cells is diagnostic of the starburst amacrines.

Our results indicate that early in development ganglion cells and cholinergic amacrine cells participate in a functional synaptic network that produces the retinal waves. Experimentally, waves could be induced by depolarization by means of activation of nAChRs, whereas curare blocked the

spread of excitation away from a site of depolarization. These observations imply that the propagation of retinal waves requires synaptic transmission mediated by the cholinergic amacrine cells. Several models, not necessarily mutually exclusive, have been proposed for the way in which the waves might spread in a network of ganglion and amacrine cells (*30*). In an "amacrine-propagated" model, excitation could spread directly between amacrine cells (not all of which need even be cholinergic) and then could be "read-out" by ganglion cells via cholinergic inputs. In this model, at least some amacrine cells also must express nAChRs because in the presence of curare, all increases in $[Ca^{2+}]_i$ in amacrine cells are abolished (*31*). In a feedback model, excitation could be relayed from amacrine to ganglion cells (by cholinergic transmission) and then back to other amacrine cells (or ganglion cells) by gap junctions that, on the basis of tracer coupling studies, are presumed to be present between ganglion and amacrine cells at these ages (*32*). Although our observations imply that cholinergic synaptic transmission is required for wave propagation, it could possibly also participate in wave initiation. Because, in the presence of curare, all changes in $[Ca^{2+}]_i$ in amacrine and ganglion cells are abolished, either ACh is required—possibly released spontaneously from a small subset of amacrine cells—or some other process that induces a change in $[Ca^{2+}]_i$ below our detection limit is necessary to initiate a wave.

The spontaneous activity in the retina generates action potentials that are sent to other structures in the visual system (*33*) and may be critical for development of visual system circuitry (*8*, *34*). Proposed models imply that the spatio-temporal pattern, not the overall level of activity, is required for the development of these early circuits (*35*). In addition to providing near-neighbor correlations among cells in the same eye (*6*), the large but finite spatial extent of the wavefronts defining the domains and the long and variable interval between successive waves within a particular region of the retina could also have functional significance for the patterning of connectivity more centrally. Moreover, the presence of correlated activity within the retinal circuits themselves could act in shaping local circuits (*9*), as has been postulated for the developing cerebral cortex (*1*) and spinal cord (*3*). Thus, although the cellular basis for generating the correlations appears to differ in detail, the nervous system can apparently use a variety of different strategies to generate correlated activity necessary for the shaping of precise circuitry.

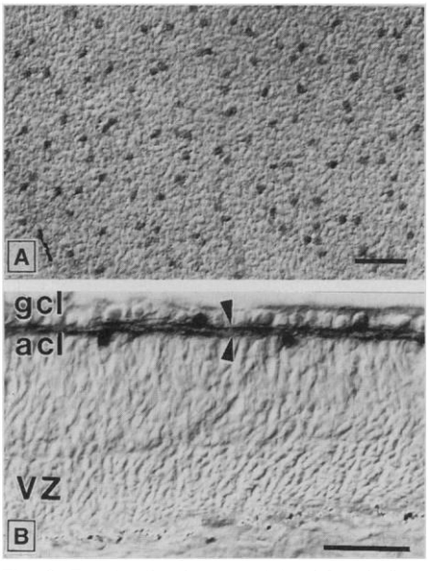

Fig. 6. Ferret retina immunostained for choline-acetyltransferase (ChAT) observed with Nomarski optics. (**A**) P2 ferret retina whole mount. (**B**) Transverse section through a P8 ferret retina. Abbreviations: acl, amacrine cell layer; gcl, ganglion cell layer; and VZ, ventricular zone. Scale bar, 50 μm for both (A) and (B).

REFERENCES

1. R. Yuste, D. A. Nelson, W. W. Rubin, L. C. Katz, *Neuron* **14**, 7 (1995); K. Kandler, L. C. Katz, *Curr. Opinion Neurobiol.* **5**, 98 (1995).
2. R. O. L. Wong, *Curr. Opinion Neurobiol.* **3**, 595 (1993); N. C. Spitzer, *Trends Neurosci.* **17**, 115 (1994); W. R. Lippe, *J. Neurosci.* **14**, 1486 (1994).
3. M. O'Donovan *et al.*, *J. Exp. Zool.* **261**, 261 (1992); X. Gu and N. C. Spitzer, *Nature* **375**, 784 (1995).
4. C. S. Goodman and C. J. Shatz, *Cell* **72**, 77 (1993); M. Constantine-Paton, H. T. Cline, E. Debski, *Annu. Rev. Neurosci.* **13**, 129 (1990); H. T. Cline, *Trends Neurosci.* **14**, 104 (1991).
5. L. Maffei and L. Galli-Resta, *Proc. Natl. Acad. Sci. U.S.A.* **87**, 2861 (1990).
6. M. Meister, R. O. L. Wong, D. A. Baylor, C. J. Shatz, *Science* **252**, 939 (1991); R. O. Wong, M. Meister, C. J. Shatz, *Neuron* **11**, 923 (1993).
7. J. S. Tootle, *J. Neurophysiol.* **69**, 1645 (1993).
8. C. J. Shatz and M. P. Stryker, *Science* **242**, 87 (1988).
9. S. R. Bodnarenko and L. M. Chalupa, *Nature* **364**, 144 (1993); E. Sernagor and N. M. Grzywacz, *Soc. Neurosci. Abstr.* **20**, 1470 (1994).
10. R. O. L. Wong, A. Chernjavsky, S. J. Smith, C. J. Shatz, *Nature* **374**, 716 (1995).
11. Retinas were isolated from newborn (P0-P10) ferrets that had been deeply anesthetized with halothane and then decapitated. All procedures were performed in artificial cerebrospinal fluid (ACSF, 119 mM NaCl, 2.5 mM KCl, 1.3 mM $MgCl_2$, 1.0 mM KH_2PO_4, 2.5 mM $CaCl_2$, 26.2 mM $NaHCO_3$, 11 mM D-glucose). Solutions were buffered with $NaHCO_3$ and oxygenated with a mixture of 95% O_2 and 5% CO_2. The retinas were placed (ganglion cell layer up) in a temperature-controlled chamber (31° to 34°C; Medical Systems) mounted on a stage of either an inverted microscope (Nikon, Diaphot 300) or an upright microscope (Technical Instruments) and continuously perfused.
12. Isolated retinas were labeled with fura-2AM: 50 μg of fura-2AM in 50 μl of 1% (w/v) pluronic acid in dimethyl sulfoxide (DMSO). The volume was increased to 5 ml with ACSF (final fura concentration was 10 μM). The retinas were incubated at 30°C in the labeling solution for 1 to 4 hours in an oxygenated chamber. All experiments were conducted with 380-nm illumination, and either a 6.3× (Zeiss Neofluor) or 10× water immersion (Nikon) objective. Images were acquired with a SIT camera (Dage, MTI 300). Initially, a background frame was acquired, which was then subtracted on a pixel-by-pixel basis from all subsequent images to create difference images. The background frame and subsequent frames were averaged over four video frames. Movies of the changes in fluorescence were acquired directly onto Hi 8 videotape (Sony) with Metamorph Software (Universal Imaging). The images were then accessed by a Macintosh computer with NIH image and analyzed with an "object selection algorithm" in Adobe Photoshop, which defines objects on the basis of the gray scale similarities of adjacent pixels. We defined domains as the region of constant fractional change in fluorescence ($\Delta F/F$) induced by the waves. The accuracy of the object selection algorithm depends on the ratio of the signal-to-noise of the individual waves, which is determined by the magnitude of $\Delta F/F$. In general, if the magnitude of the $\Delta F/F$ response is more than 5%, then the algorithm would define domain boundaries in a reproducible way. This was the situation of the vast majority of domains we analyzed. When waves induced a $\Delta F/F$ response less than 5%, the definition of the domain boundaries became less reliable. By applying the algorithm repeatedly to the same wave, we estimate the error in determining domain size and shape to be within 10%. In addition, the correlation between the changes in fluorescence and the presence of synaptic currents recorded simultaneously from the ganglion cells (Fig. 3B) is sufficient to infer that this determination of boundaries based on fluorescence measurements accurately reflects the distribution of neural activity.

12a. The videotape is available at http://science-mag.aaas.org/science/feature/beyond/#feller

13. The pressure pulse ranged from 50 to 200 ms from a pipette tip of 5 to 10 μm at 5 to 7 psi. These conditions depolarize a localized group of cells [P. Lukasiewicz and F. S. Werblin, *J. Neurosci.* **10**, 210, (1990)]. The pressure-ejected solution consisted of ACSF where Na^+ has been replaced with an equimolar amount of K^+ (120 mM K^+ final concentration). Pressure ejections were directed at discontinuities in the tissue to allow for access to cell processes.
14. Cells in the retinal ganglion cell layer were exposed by making microscopic tears in the nerve fiber layer with a patch pipette tip and were visualized with conventional brightfield microscope optics with an Olympus 40× water immersion objective. Membrane currents were measured in the whole-cell configuration of the patch clamp technique. The intracellular solution consisted of 5 mM KCl, 96 mM potassium gluconate, 5 mM $MgCl_2$, 4 mM ATP, 0.3 mM GTP, 38 mM Hepes, 0-1 mM EGTA, pH 7.25. For reversal potential experiments, 100 mM cesium gluconate replaced the KCl and potassium gluconate, and 1 mM lidocaine *N*-ethyl bromide quaternary salt (QX-314, Research Biochemicals International) was added to the solution. Voltage clamp recordings were done with an Axopatch 200A amplifier (Axon Instruments). Unless noted otherwise, the holding potential was −60 mV. Continuous recordings of spontaneous synaptic currents were filtered at 1 kHz, digitized at 2.5 kHz (Digidata 1200), and stored with the use of pClamp 6.0 software (Axon Instruments).
15. B. Rorig and R. Grantyn, *Neuroreport* **5**, 1197 (1994).
16. R. H. Masland and A. D. Ames, *J. Neurophysiol.* **39**, 1220 (1976); E. Sernagor and N. M. Grzywacz, *Ophthalmol. Vis. Sci. (suppl.)* **35**, 2125 (1994).
17. Z. Zhang, S. Vijayayaghavan, D. S. Berg, *Neuron* **12**, 167 (1994).
18. P. B. Sargent, *Annu. Rev. Neurosci.* **16**, 403 (1993); D. S. McGehee and L. W. Role, *Annu. Rev. Physiol.* **57**, 521 (1995).
19. E. Aizenman, R. H. Loring, S. A. Lipton, *Brain Res.* **517**, 209 (1990); D. E. Hamassaki-Britto *et al.*, *J. Comp. Neurol.* **347**, 161 (1994).
20. R. G. Pourcho, *Brain Res.* **198**, 33 (1980); J. L. Mosinger, S. Yazulla, K. M. Studholme, *Exp. Eye Res.* **42**, 631 (1986); H. Wassle and M. H. Chun, *J. Comp. Neurol.* **279**, 43 (1989); S. Yazulla, *Neurosci. Res. Suppl.* **2**, S147 (1985).

21. S. Heaulme *et al.*, *Brain Res.* **384**, 224 (1986); C. A. Kittila and S. C. Massey, *J. Neurophysiol.* **73**, 703 (1995); C. J. Dong, S. A. Picaud, F. S. Werblin, *J. Neurosci.* **14**, 2648 (1994).
22. These inward rectifying and nonrectifying curves could be reproduced by measuring an individual ganglion cell's response to pressure ejection of ACh (n = 5 cells from two retinas) or ACh plus GABA (n = 2 cells from 1 retina), respectively (D. P. Wellis, M. B. Feller, C. J. Shatz, F. S. Werblin, unpublished data).
23. There is evidence in rat hippocampus that *d*-tubocurarine can act as a weak competitive antagonist for $GABA_A$ receptors [F. J. Lebeda, J. J. Hablitz, D. Johnston, *J. Neurophysiol.* **48**, 622 (1982)], implying that our results could be due to a pharmacological blockade of $GABA_A$ receptors and not neuronal nAChRs. However, it has been shown that nicotine has no cross-reactivity with $GABA_A$ receptors [V. E. Wotring and W. Yoon, *Neuroscience* **67**, 293 (1995)], implying that the blockade of waves we see in the presence of nicotine is due to desensitization of nAChRs. This conclusion, combined with the rectifying characteristics of I-V relationship of the compound PSCs seen in the presence of SR95531 implies that the *d*-tubocurarine is acting directly on nAChRs. In addition, in intermediate lobe cells of the porcine pituitary, although the $GABA_A$ antagonist bicuculline acts as a competitive antagonist at nAChRs, SR95531 does not [Z. W. Zhang and P. Feltz, *Br. J. Pharmacol.* **102**, 19 (1991)]. In view of the specific effect that SR95531 has on the chloride contribution to the periodic compound PSCs, we can conclude SR95531 acts specifically on $GABA_A$ receptors. Although $GABA_A$ activated Cl^- conductances are triggered during a wave, their contribution to the propagation of the wave may depend critically on how much these conductances excite the cell. In several kinds of immature neurons, GABA can have excitatory effects [K. J. Staley, B. L. Soldo, W. R. Proctor, *Science* **269**, 977 (1995); E. Cherubini, J. L. Gaiarsa, Y. Ben-Ari, *Trends Neurosci.* **14** (12), 515, (1991)]; however, the GABA response has not been characterized for retinal ganglion cells.
24. R. H. Masland and M. Tauchi, *Trends Neurosci.* **9**, 218 (1986); D. I. Vaney, *Progr. Retinal Res.* **9**, 49 (1990); E. V Famiglietti, Jr., *Vision Res.* **23**, 1265 (1983); E. V. Famiglietti, *J. Neurosci.* **5**, 562 (1985).
25. M. Ariel and N. W. Daw, *J. Physiol. (London)* **324**, 161 (1982).
26. E. V. Famiglietti, *J. Comp. Neurol.* **309**, 40 (1991); C. Brandon, *Brain Res.* **426**, 119 (1987).
27. T. J. Millar and I. G. Morgan, *Neurosci. Lett.* **74**, 281 (1987).
28. N. Brecha, D. Johnson, L. Peichl, H. Wassle, *Proc. Natl. Acad. Sci. U.S.A.* **85**, 6187 (1988); T. Kosaka, M. Tauchi, J. L. Dahl, *Exp. Brain Res.* **70**, 605 (1988); D. M. O'Malley, J. H. Sandell, R. H. Masland, *J. Neurosci.* **12**, 1394 (1992); M. J. Neal, J. R. Cunningham, P. H. Hutson, J. E. Semark, *Neurochem. Int.* **20**, 43 (1992).
29. Isolated retinas were post-fixed for 30 minutes in 4 percent paraformaldehyde in 0.1 M sodium phosphate buffer (pH 7.4), and stained for ChAT as described [T. Voigt, *J. Comp. Neurol.* **248**, 19 (1986)] with the following modifications. We used an affinity purified goat polyclonal antibody to ChAT (Chemicon), visualized with an avidin biotin reaction combined with 3,3′-diaminobenzidine (DAB) and 0.1 to 0.2% $NiCl_2$. Some retinas were sectioned (25 μm) transversely on a cryostat and subjected to the same protocol. Seven retinas between P2 and P8 were studied.
30. A recently proposed model [P. Y. Burgi and N. M. Grzywacz, *J. Neurosci.* **14**, 7426 (1994)] was based on the assumption that the spread of excitation was through extracellular potassium. This model is inconsistent with our results because blocking K^+ currents with intracellular Cs^+ had no effect on the periodic compound PSCs. In addition, the reversal potential for the compound PSCs was not consistent with a K^+ conductance.
31. This model is consistent with the observations that amacrine cells in the developing rabbit retina have functional nAChRs [R. O. Wong, *J. Neurosci.* **15**, 2696 (1995)] and that, in the developing chick retina, amacrine cells have the α-bungarotoxin–insensitive form of the neuronal nAChR [D. E. Hamassaki-Britto *et al.*, *J. Comp. Neurol.* **347**, 161 (1994); K. T. Keyser *et al.*, *J. Neurosci.* **13**, 442 (1993)].
32. A. A. Penn, R. O. L. Wong, C. J. Shatz, *J. Neurosci.* **14**, 3805 (1994).
33. C. J. Shatz, *Proc. Nat. Acad. Sci. U.S.A.* **93**, 602 (1996); R. Mooney, A. A. Penn, R. Gallego, C. J. Shatz, unpublished data.
34. B. Chapman and M. P. Stryker, *J. Neurosci.* **13**, 5251 (1993).
35. C. von der Malsburg, *Kybernetik* **14**, 85 (1973); R. Linsker, *Proc. Natl. Acad. Sci. U.S.A.* **83**, 8390 (1986); K. D. Miller, J. B. Keller, M. P. Stryker, *Science* **245**, 605 (1989).
36. We thank D. Bentley for lending us a SIT camera, R. Yakura for assistance in the image processing, E. M. Messersmith for assistance on the histology, and R. Gallego and P. Dayan for useful discussions. Supported by NSF IBN 93-19539; March of Dimes; NIMH 48108 (C.J.S.); U. C. Berkeley Miller Fellowship (M.B.F.); NIH grants GM07048 (D.S.), EY00561 (F.S.W.), and EY06292 (D.P.W.); and of the Howard Hughes Medical Institute (C.J.S.).

26 December 1995; accepted 10 April 1996

Polyclonal Origin of Colonic Adenomas in an XO/XY Patient with FAP

M. R. Novelli,* J. A. Williamson, I. P. M. Tomlinson, G. Elia, S. V. Hodgson, I. C. Talbot, W. F. Bodmer, N. A. Wright

It is widely accepted that tumors are monoclonal in origin, arising from a mutation or series of mutations in a single cell and its descendants. The clonal origin of colonic adenomas and uninvolved intestinal mucosa from an XO/XY mosaic individual with familial adenomatous polyposis (FAP) was examined directly by in situ hybridization with Y chromosome probes. In this patient, the crypts of the small and large intestine were clonal, but at least 76 percent of the microadenomas were polyclonal in origin.

Investigations of clonality in the normal intestinal mucosa have centered on the examination of laboratory mice (*1–3*). In the neonatal mouse, intestinal crypts are polyclonal, but through a process known as "purification," crypts become monoclonal by the time mice are 2 weeks old (*4*). In the normal human intestine, investigation has been limited by the lack of suitable markers of clonality. Clonality studies are of great relevance to our understanding of the process of tumorigenesis. Proponents of mutational theories of tumor development suggest that tumors arise from a series of mutations occurring in one cell and its progeny (*5–7*). Others have argued that tumors are not clonal in origin but require the interaction of multiple cells (*8, 9*) and that outgrowth of a dominant clone during subsequent development accounts for their apparent monoclonality.

It is possible to differentiate between XY cells and XX or XO cells by in situ hybridization with chromosome-specific probes; thus, the Y chromosome can be used to determine patch size and tissue clonality, as in XX/XY chimeric mice (*10*). To investigate clonality in the human intestine, we studied tissue from an XO/XY mosaic individual of male phenotype who, by coincidence, also had familial adenomatous polyposis (FAP). This was a serendipitous discovery, as the chance of finding such an individual is probably less than one in a hundred million. The clinical diagnosis of FAP was confirmed by mutation analysis of the patient's *APC* gene: A protein truncation test and subsequent sequence analysis (*11*) revealed a germline frameshift mutation at codon 1309. The patient had undergone a prophylactic total colectomy at 32 years of age, from which paraffin-embedded material was available.

We first performed karyotyping and fluorescent in situ hybridization (FISH) (*12*), using the Y chromosome-specific probes cY97 and pDP105 (*13*), on the patient's peripheral blood lymphocytes (PBLs). These tests confirmed that he was a mosaic and also showed the Y chromosome to be dicentric. The karyotype was 45,X/46,X, dic(Y)(Ypter → cen → Yq11.23:: Yp11.3 → cen → Yq11.23). FISH demonstrated that approximately 20% of the PBLs were XO.

Nonisotopic in situ hybridization (NISH) (*14*) was then performed on histological sections of the small and large intestine, with the use of the Y chromosome–

M. R. Novelli, I. P. M. Tomlinson, W. F. Bodmer, Cancer Genetics Laboratory, Imperial Cancer Research Fund (ICRF) Laboratories, Post Office Box 123, 44 Lincoln's Inn Fields, London WC2A 3PX, UK.
J. A. Williamson, Human Cytogenetics Laboratory, ICRF, London WC2A 3PX, UK.
G. Elia, Histopathology Unit, ICRF, London WC2A 3PX, UK.
S. V. Hodgson and I. C. Talbot, ICRF Colorectal Unit, Saint Marks and Northwick Park National Health Service Trust, Watford Road, Harrow, Middlesex, HA1 3UJ, UK.
N. A. Wright, Histopathology Unit, ICRF, London WC2A 3PX, and Department of Histopathology, Royal Postgraduate Medical School, Hammersmith Hospital, Du Cane Road, London W12 0HS, UK.
*To whom correspondence should be addressed.